Results and Discussion

Neither a weight loss ΔW nor a thickness loss Δt was detected for coatings Teflon, Kapton, or glass resin coatings, and no weight loss was detected for silicone, polyurethane, or the substrate aluminum (specimen 4, Table 2). The very hard coatings (flame-sprayed NiAl, plasma-sprayed Al_2O_3, and glass reference slides) and the soft H-10 coating (highly pigmented) did experience significant ΔW's and Δt's. At a given ρ_d*, the change in θ from 45° to 90° had no effect on ΔW except for the Al_2O_3 and the glass reference slide, both of which had greater weight losses at 90°. Increasing ρ_d* from 1.0 to 1.45 with $\theta = 90°$ did not cause any appreciable increase in ΔW of any materials tested, including the glass reference materials. Increasing T_e from 2 to 4 hr, with about the same ρ_d* (1.5) and a 90° orientation, did increase ΔW for the flame and plasma-sprayed coatings and the H-10 coating. Except for the glass reference materials, increasing T_e from 2 hr to 4 hr did not produce a 100% increase in ΔW for the hard materials.

The α_s and ϵ_{t_n} changes are given in Table 3. With the exception of the flame-sprayed NiAl and NiAl + ZrO_2, and the grit-blasted aluminum, a large increase in α_s occurred when ρ_d* was increased from 1.0 to 1.5 or T_e was increased from 2 hr to 4 hr. The flame-sprayed coatings, originally porous and rough, were smoother after testing. Their increased α_s may be explained by the possibility of silica dust pickup that did not get removed by the cleaning procedure. The metallized films (aluminum-Teflon, gold-Teflon and gold-Kapton) increased in α_s as the exterior surface was etched or contaminated (silica dust pickup); this produced a diffuse surface coating over the metallized film. The unpigmented glass resin was etched by the dust, thereby producing a diffuse surface. The grit-blasted aluminum (6061-T6 alloy) surface became smooth. These results for the selected window materials and mirrors are plotted as reflectance or transmittance vs T_e in Fig. 3 for two wavelengths. In Fig. 3a, the difference between the upper (DST) curve and the lower (DT) curve in Fig. 3 is the amount of incident light usable to form an image. For $T_e \geq 15$ min, less than 15% of the incident light reaches the image. The initial test data (Fig. 3) indicate that the harder alumino-silicate is a better window material than the fused silica for the sand/dust erosion environment. The alumino-silicate has a Knoop hardness (100-g load) of 595 kg/mm² as compared to 560 kg/mm² for fused silica. For $T_e = 5$ min, the difference between the DST and DT values for the alumino-silicate is 56%, as compared to 46% for the fused silica material.

No resolution measurements were made on the mirrors. If the mirror reflectance and scattering for Figs. 3b and 3c are interpreted in the same manner as for window transmittance, it is evident that little light is available for formation of an image. The mirrors were slightly less degraded in the infrared (1750) than in the visible region (550). The second-surface mirrors (Fig. 3b) were physically more durable than the first-surface mirrors (Fig. 3a), but it should be noted that incident light passes through the damaged front surface of a second-surface mirror twice.

Conclusions

The erosion of the hard materials (flame-sprayed coatings and the glass references) increased as exposure time and dust density increased. The more resilient coatings (Teflon, Kapton, polyurethane, elastomeric silicone, etc.) did not exhibit any weight loss under any test conditions. Large increases in α_s, due to dust pickup and/or changes in surface roughness, were experienced by all coatings except the flame-sprayed nickel aluminide-type coatings. The NiAl-type coatings were the only ones to exhibit a decrease in ϵ_{t_n}; all other coatings exhibited either increased ϵ_{t_n} or no change in ϵ_{t_n}. Consequently, even though most of the coatings suffered an increase in α_s, the α_s/ϵ_{t_n} ratio for a number of them remained in the useful 0.40–0.70 range.

The specimens with initially lower α_s/ϵ_{t_n} (H-10 and plasma-sprayed Al_2O_3) had the smallest change in α_s/ϵ_{t_n}, possibly because the more resilient surfaces retain impacted silica instead of eroding away. The H-10 and plasma-sprayed Al_2O_3 erode and thus always present a clean surface. Since the solar constant for Mars is 190/Btu/hr-ft² (less than one-half that of Earth), a coating with $\alpha_s/\epsilon_{t_n} \simeq 0.70$ (with $\epsilon_{t_n} = 0.80$) could possibly be utilized on a vehicle without having it overheat when on the Martian surface; thus, it appears probable that further work will produce a suitable thermal control coating for a vehicle operating on the surface of Mars.

For window materials exposed more than 10 min and mirrors exposed more than 5 min, the amount of radiation available for image formation is significantly decreased. This results in a serious loss in resolution, especially at low contrast levels. The brightness of an image, as observed with a first surface mirror, was less than 10% of the true brightness. For windows exposed more than 10 min, the brightness was less than 15% in the visible (550) and less than 25% in the infrared (1750) regions.

References

[1] Stone, I., "Atmospheric Data to Alter Voyager Design," *Aviation Week and Space Technology*, Vol. 83, No. 21, Nov. 22, 1965.

[2] Christian de Wys, E., "The Surface of Mars," 1968, Jet Propulsion Lab., Pasadena, Calif.

[3] Hertzler, R. G., "Behavior Characteristics of Simulated Martian Sand and Dust Storms," Rept. E720, Aug. 1966, McDonnell Aircraft Co., St. Louis, Mo.

[4] Hertzler, R. G., Wang, E. S. J., and Wilbers, O. J., "Martian Sand and Dust Storm Experimentation," *Journal of Spacecraft and Rockets*, Vol. 4, No. 2, Feb. 1967, pp. 284–286.

[5] "Mars Engineering Model Parameters for Mission and Design Studies," May 1968, NASA.

[6] Rusert, E. L. and Wilbers, O. J., "Effects of Spacecraft Sterilization Procedures and Mars Environment on Thermal Control Coatings," *The Effects of Space Environment on Materials*, Vol. 11, Western Periodicals, North Hollywood, Calif., April 1967, pp. 63–73.

A Study of the Nonlinear Rolling Motion of a Four-Finned Missile

PETER DANIELS*
Naval Weapons Laboratory, Dahlgren, Va.

Nomenclature

C_l = aerodynamic rolling moment coefficient
C_{l_p} = aerodynamic roll damping coefficient
$C_{l\delta}$ = C_l derivative due to fin cant
$C_{l_{4\gamma}}$ = induced rolling moment coefficient for a four-finned missile
d = missile reference diameter
I_x = axial moment of inertia
N = number of fins
p = spin rate
Q = dynamic pressure
S = reference area
V = missile velocity
α = angle of attack
γ = angle between reference fin and normal component of missile velocity
δ = fin cant angle

Received October 22, 1969; revision received January 12, 1970. Acknowledgement is due C. J. Cohen, Research Associate for the Warfare Analysis Department, who first suggested that the roll damping at high angles of attack could be expressed as a cubic. Equation (5) is also due to him.

* Research Scientist, Warfare Analysis Department.

Introduction

ANALYSIS of missile dynamics has been developed to a high degree for cases where the differential equations of motion, including aerodynamic terms, can be linearized. This approach is reasonably accurate when the missile's angle of attack (α) is small. However, when α is large, nonlinear effects become apparent and must be considered in accurate six-degree-of-freedom trajectory analysis. For a finned missile rolling at fixed α, the roll moment is periodic and therefore nonlinear. To gain a better understanding of the effects of this nonlinear moment, an experimental study was conducted. This Note presents the results of that study.

Nonlinear Rolling Motion

Nicolaides[1,2] found that freely rolling finned missiles exhibit five characteristic rolling motions (Fig. 1) that depend upon α and fin cant angle δ. In linear rolling motion, the roll moment is proportional to δ and rolling velocity and is independent of α. "Slow-down" is an effect of yaw such that the roll moment caused by δ becomes less effective relative to the damping torque. "Lock-in" occurs when the induced moment caused by the roll angle, relative to the normal component of velocity, balances the roll moment caused by δ. At higher α's, the lock-in becomes unstable and "break-out" occurs. After break-out, even with $\delta = 0$, roll "speed-up" can occur. Apparently, the roll torque due to roll rate becomes positive at low roll rates for α's above lock-in.

In the classical linear theory of rolling motion the total aerodynamic roll coefficient for a particular α is

$$C_l(\delta,p) = C_{l\delta}\delta + C_{l_p}pd/(2V) \quad (1)$$

Nicolaides[1] postulated, and it was later shown[2] that there existed a periodic (thus, nonlinear) static roll coefficient ($C_{l_{N\gamma}} \sin N\gamma$) which could account for roll lock-in. Consequently, the differential equation more recently used[1-3] to describe the free flight rolling motion of four-finned missiles at a particular α is

$$I_x\dot{p}/QSd = C_{l\delta}(\alpha)\delta + C_{l_p}(\alpha)pd/2V + C_{l_{4\gamma}}(\alpha)\sin 4\gamma \quad (2)$$

For the wind-tunnel case with freedom only in roll, $\dot{\gamma} = p$, and Eq. (2) may be written as

$$I_x\ddot{\gamma}/QSd = C_{l\delta}(\alpha)\delta + C_{l_{\dot\gamma}}(\alpha)\dot{\gamma}d/2V + C_{l_{4\gamma}}(\alpha)\sin 4\gamma \quad (3)$$

However, at higher α's where the lock-in becomes unstable and speed-up occurs, this approximate equation cannot even qualitatively describe the phenomena. Therefore, static and dynamic wind-tunnel tests were conducted to provide the information required to construct a more exact nonlinear rolling motion theory. The basic finner, a standard Navy research configuration (Fig. 2), was tested in the Naval Ship Research and Development Center's 7 × 10-ft subsonic wind tunnel.

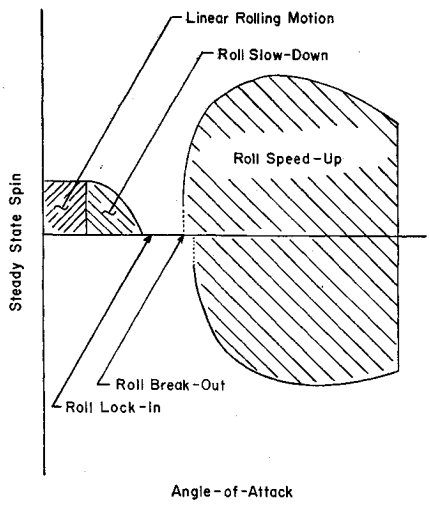

Fig. 1 Characteristic rolling motions of cruciform finned missiles.

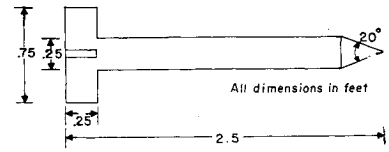

Fig. 2 Schematic of basic finner model.

The static force data, measured with a strain-gage roll balance, showed that the induced static rolling moment $C_l(\gamma)$ is sinusoidal only at very low α's; at higher α's, it approaches a more saw-toothed form as illustrated in Fig. 3. A least-squares fit of a Fourier sine series was made to the $C_l(\gamma)$ data for $0 \leq \alpha \leq 90°$. Figure 4 shows the results for the higher-order terms in the series,

$$\sum_{K=1}^{4} C_{l_{4K\gamma}} \sin 4K\gamma$$

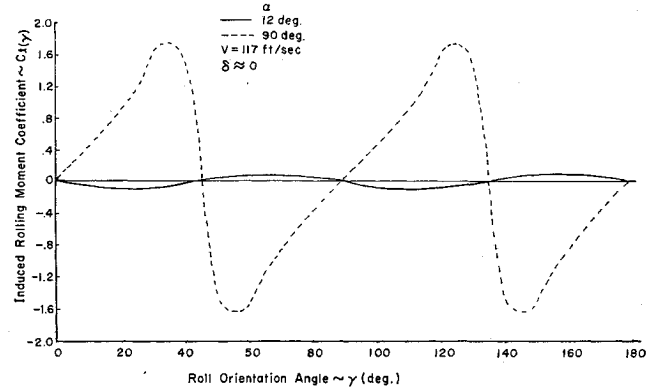

Fig. 3 Induced rolling moment vs roll orientation angle for basic finner model measured in incompressible flow.

Data obtained at other subsonic velocities show these same characteristics. With these new higher-order terms, Eq. (3) becomes

$$I_x\ddot{\gamma}/QSd = C_{l\delta}(\alpha)\delta + \sum_{K=1}^{\infty} C_{l_{4K\gamma}}(\alpha)\sin 4K\gamma + C_{l_{\dot\gamma}}(\alpha)\dot{\gamma}d/2V \quad (4)$$

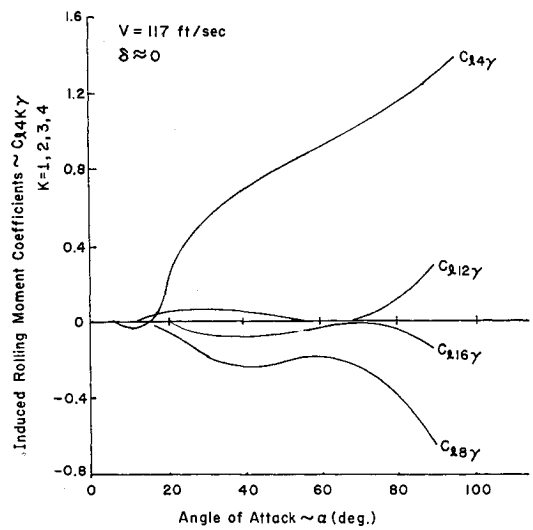

Fig. 4 Induced rolling moment coefficients vs angle of attack for basic finner in incompressible flow.

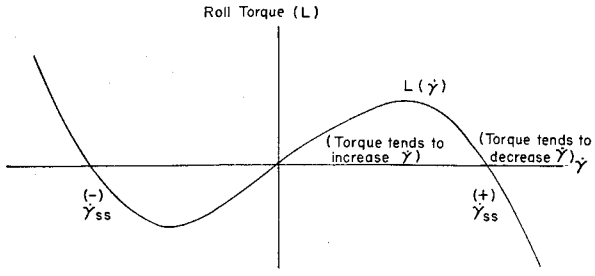

Fig. 5 Hypothetical damping function which can account for roll break-out and roll speed-up.

However, Eq. (4) still cannot describe the roll break-out and speed-up phenomena. When the basic finner model is released from rest and allowed to roll freely on a string-mounted, internal, air bearing, it exhibits unstable oscillations about a strong roll trim point at large α's when the rolling velocity is small, implying that the torque due to roll rate is positive. It then "breaks-out" and "speeds-up" to a steady-state rate $\dot{\gamma}_{ss}$, sometimes in the direction of, and sometimes opposed to, the cant. At this point the rolling torque as a function of $\dot{\gamma}$ must have a real root with negative slope, since overspinning the missile results in negative damping. We, therefore, conclude that if the damping torque is continuous with $\dot{\gamma}$, it must have roughly the cubic form shown in Fig. 5.

Figure 6 shows $\dot{\gamma}_{ss}$ vs α for the basic finner missile with and without fin cant. When $\delta \simeq 0$, the dual steady-state spin rates are nearly equal for the particular α. When $\delta \simeq 3°$ and in the region of unstable oscillations and break-out, there exists a large region where break-out is possible only in the positive direction of spin. At slightly higher α's, where break-out can occur in either direction, $\dot{\gamma}_{ss}$ is usually slightly higher in the positive direction of spin.

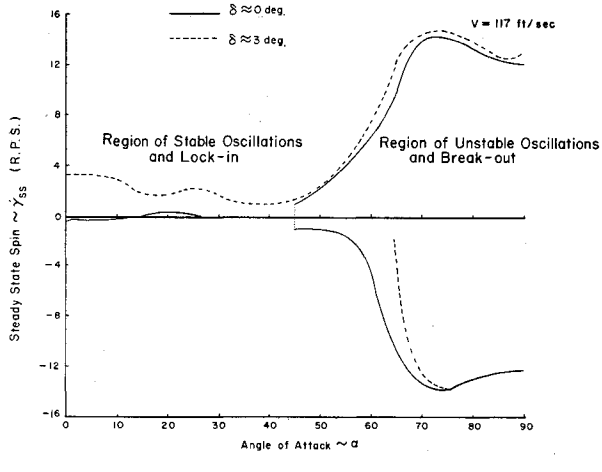

Fig. 6 Steady-state spin vs angle of attack for the basic finner with and without fin cant.

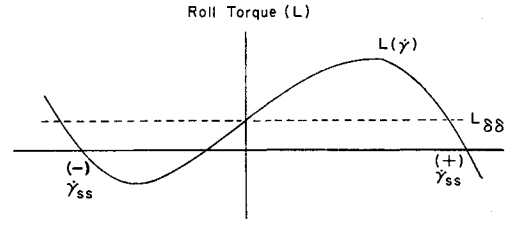

Fig. 7 Superposition of roll moment due to fin cant on cubic damping function.

These rolling characteristics can also be explained in terms of the present nonlinear theory. When the missile is circulating (e.g., $\dot{\gamma}$ does not oscillate) the roll rate approaches a quasi-steady state, and the contribution of the periodic torque may then be neglected. If we then consider a simple superposition of a roll torque due to fin cant ($L_\delta\delta$) on the cubic form of damping shown in Fig. 7, the displacement produces an increase in the positive $\dot{\gamma}_{ss}$ and a decrease in the negative $\dot{\gamma}_{ss}$. Moreover, if the moment due to fin cant is sufficiently large compared to the damping moment, only break-out and speed-up with positive spin is possible, since the negative spin is damped.

Now if the damping is also analytic with spin, we may express it in the form of a Taylor series whose coefficients depend on odd powers of $\dot{\gamma}$. The Fourier series and Taylor series can be combined into a more general differential equation that contains mixed terms

$$\ddot{\gamma} I_x/(QSd) = C_{l\delta}(\alpha)\delta + \sum_{m,K} C_{l_{mK}}(\alpha)\dot{\gamma}^m \sin(4K\gamma + \tfrac{1}{2}m\pi) \tag{5}$$

This is the general form which, when $\delta = 0$, has the symmetry property $\ddot{\gamma}(-\gamma,-\dot{\gamma}) = -\ddot{\gamma}(\gamma,\dot{\gamma})$.

Conclusions

The results of this study indicate that: 1) the static aerodynamic roll moment is most naturally described by a Fourier series over the angle of attack (α) range of 0 to 90°; 2) at low α's the rolling motion of a four-finned missile conforms to a second-order differential equation that contains a linear damping term, whereas at higher α's, the damping must be at least cubic in nature; and 3) the differential equation of rolling motion proposed herein is needed to describe more accurately the rolling motion of four-finned missiles.

References

[1] Nicolaides, J. D., "An Hypothesis for Catastrophic Yaw," TN-18, Sept. 1955, Bureau of Ordnance, U.S. Navy, Washington, D. C.

[2] Nicolaides, J. D., "Missile Flight and Astrodynamics," TN-100A 1959–1961, Bureau of Naval Weapons, Washington, D. C.

[3] Cohen, C. J. and Werner, D., "A Formulation of the Equations of Motion of a Four-Finned Missile," NAVORD Rept. 5133, Sept. 27, 1956, Naval Proving Ground, Dahlgren, Va.